

Fleischmann, M. and M. Miles. *The "Instrument Function" of Isoperibolic Calorimeters; Excess Enthalpy Generation due to the Parasitic Reduction of Oxygen.* in *Tenth International Conference on Cold Fusion*. 2003. Cambridge, MA: LENR-CANR.org. This paper was presented at the 10th International Conference on Cold Fusion. It may be different from the version published by World Scientific, Inc (2003) in the official Proceedings of the conference.

The "Instrument Function" of Isoperibolic Calorimeters; Excess Enthalpy Generation due to the Parasitic Reduction of Oxygen.

M. Fleischmann  
Bury lodge, Duck Street, Tisbury, Salisbury, Wilts., SP3 6LJ, U.K.  
M.H. Miles  
Department of Chemistry, University of La Verne, CA 91750, U.S.A.

Two criticisms which are frequently advanced to counter observations of the generation of excess enthalpy in the cathodic polarisations of Pd-based electrodes in D<sub>2</sub>O-based electrolytes (e.g. see (1), (2)) are usually based on the assertion that the isoperibolic calorimeters used in these studies are imprecise and inaccurate. Furthermore, any excess enthalpy generation is then attributed to the reduction of electrogenerated oxygen although such assertions have not been accompanied by appropriate measurements. There is naturally a link between these two assertions.

The first step in the development of any investigative methodology should be the determination of the relevant "instrument functions" of the instrumentation used, here the isoperibolic calorimeter illustrated in Fig. 1.

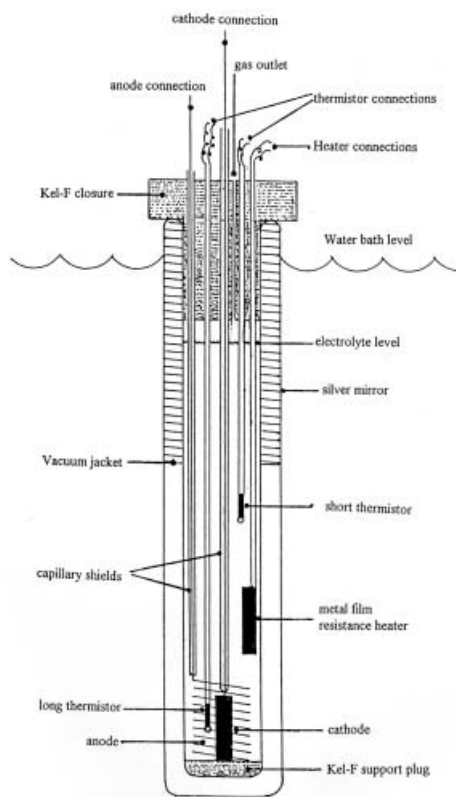


Fig 1. The Isoperibolic Calorimetric Cell.

We note the following key features of this design:

- (i) heat transfer is controlled by radiation across the vacuum gap, this heat transfer being predominantly due to the lower, unsilvered parts of the cells. The heat transfer is therefore given by the product of the Stefan-Boltzmann coefficient and the radiant surface area as has been confirmed in numerous studies. Departures from the predicted value must therefore indicate malfunctions of the cells (e.g. “softening” of the vacuum) and/or mistakes in the data analyses.
- (ii) as heat transfer is due to radiation across the gap, the thermal impedance has no “memory”. It is therefore possible to examine the non-steady state behaviour of the systems especially the response to calibration pulses supplied by the Joule resistive heaters. It is evident that this crucially important design criterion has not been understood by the many critics of “Cold Fusion” (e.g. see (3)).
- (iii) the long and narrow design of the calorimeters ensures that the contents are well mixed by the gas sparging induced by gas evolution at the anodes and cathodes. The radial and axial mixing times of the system (as revealed by tracer experiments) are ~3s and ~20s whereas the thermal relaxation time of the ICARUS-2 cell investigated in the present paper is ~5000s<sup>1,2</sup>.
- (iv) in view of (iii) the contents of the calorimeter have always been at a uniform temperature.
- (v) equally, the heat sinks (water baths) surrounding the calorimeters have always been at a uniform temperature. This has been ensured by using a combined rejection of heat to the surrounding ambient room temperature coupled to thermostatic control of the water baths. The room temperature has been itself controlled using two independent temperature controllers operated in parallel. The overall system therefore used two thermal impedances operated in series.
- (vi) the cells have always been operated in the “open mode” i.e. the products of electrolysis have been vented to the ambient.<sup>3</sup> N.M.R. measurements confirmed that this strategy (imposing continuous isotopic separation of H) ensured the maintenance of the initial isotopic composition of the electrolyte.
- (vii) the use of 0.1M LiOD/D<sub>2</sub>O ensured that there were no parasitic reactions (other than the reduction of electrogenerated oxygen) which could affect the thermal balances of the system.
- (viii) the volumes of the gases evolved agreed to within ~1% of those calculated assuming 100% Faradaic efficiency of the electrolytic reactions provided we neglected the initial parts of the measurement sequences during which there is charging of Pd-based electrodes by hydrogen isotopes. The volume of D<sub>2</sub>O required to maintain the levels of electrolyte in the cells also agreed with those calculated by Faraday’s Laws. There is therefore no possibility of invoking the large-scale recombination of the evolved gases to explain excess enthalpy generation.
- (ix) measurements of the cell and calibration currents, of the cell and bath temperatures and of the cell potentials and potentials across the resistive calibration heaters were made

---

<sup>1</sup> The differential equation representing the model of the calorimeter is non-linear and inhomogeneous (see equations A.1 and A.2 of the Appendix). The estimate of a “thermal relaxation time” is therefore approximate.

<sup>2</sup> The calorimeters used in the initial studies (1), (2) had heat transfer coefficients which exceeded the product of the Stefan-Boltzmann coefficient and the radiant surface area and this was attributed to conduction across the vacuum gap due to inadequate evacuation of the cells. It was not clear therefore whether the system should have been modelled as being “pseudo-radiative” or “pseudo-conductive” (depending on whether the conductive or radiative contribution was neglected ; for an alternative strategy see (4), (5)). The thermal relaxation time of these cells was ~3000s.

<sup>3</sup> It should be noted that this strategy avoids the introduction of large localised and fluctuating sources of heat in the gas spaces (which is a characteristic of cells fitted with catalytic recombiners).

every 300s<sup>4</sup>

(x) three calorimetric cells were maintained in each thermostat tank.

(xi) in view of the small extent of the head spaces (which contained no exposed bare metal parts), the systems could be operated in absolute safety.

### Measurements and Interpretation.

Fig. 2 gives a plot of the “raw data” (the cell temperature and input enthalpy for days 9 and 10 of the measurement cycles) carried out on a Pt cathode ( $\phi = 1\text{mm}$ ,  $\ell = 2\text{cm}$ ). These time series show small decreases with time following each perturbation due to the increase of the electrolyte concentration caused by the progressive electrolysis. In turn, this leads to a decrease in the enthalpy input and hence the cell temperature.

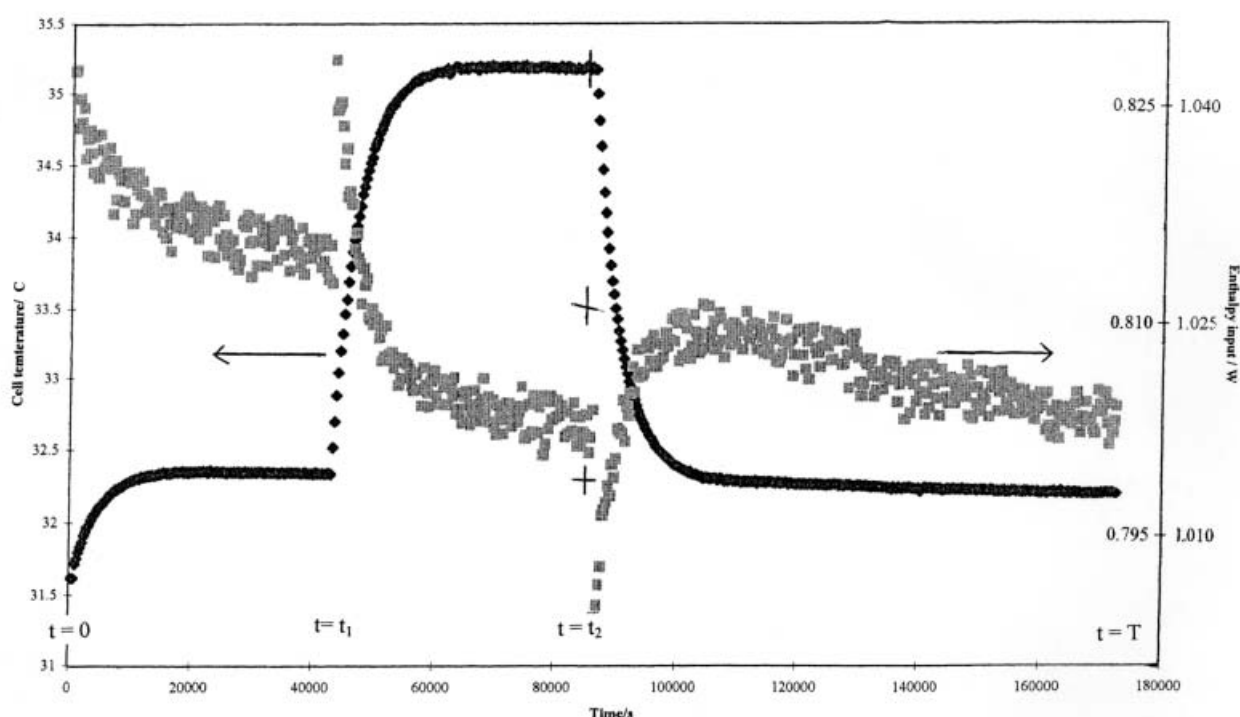


Fig 2. Plot of the "raw data" for days 9 and 10 of the "blank experiment". Pt cathode ( $\phi = 1\text{mm}$ ,  $\ell = 2\text{cm}$ ) polarised at 0.2A in 01 M LiOD/D<sub>2</sub>O. Estimates of the pseudo-radiative lower bound heat transfer coefficient,  $(k_R')_1$ , and of the pseudo-radiative true heat transfer coefficient,  $(k_R')_2$ , can be made near the end of the calibration period at  $t=t_2$ .

Two times are of special interest;  $t = t_1$  the start of the calibration period and  $t = t_2$  the end of this period. The times  $t = 0$  following the “topping up” of the cell after the previous measurement cycle and  $t = T$  the end of this cycle are of lesser interest (see further below). Estimates of the pseudo-radiative lower bound heat transfer coefficient,  $(k_R')_1$ , and of the pseudo-radiative true heat transfer coefficient,  $(k_R')_2$ , can be made near  $t = t_2$ , equations A.4 and A.6 in the Appendix. In the first of these estimates, we assume that there is no generation of excess enthalpy, hence the

<sup>4</sup> A limit on the rate of data acquisition is set by the time lags induced by the thin glass shields surrounding the thermistors,  $\sim 10\text{s}$ . (see also further below). Furthermore, it would be possible to exceed this rate of data acquisition if the time lags in the glass shields were taken into account.

designation “lower bound”; the presence of any *known* source of excess enthalpy would increase the enthalpy input and hence decrease the heat transfer coefficient. In the evaluation of  $(k_R')_2$  we also have to estimate the input power and cell temperature which would have been reached in the absence of the heater calibration. This can be done by interpolating the time series for the regions  $t < t_1$  and  $t_2 < t < T$ . The reason for stipulating  $t_1 = 12$  hours,  $t_2 = 24$  hours and  $T = 48$  hours will be self-evident. Contraction of these times to say  $t_1 = 6$  hours,  $t_2 = 12$  hours and  $T = 24$  hours inevitably lowers the precision of  $(k_R')_1$  and accuracy of  $(k_R')_2$  but, unfortunately such contractions have been the norm in most investigations carried out by other research groups.

The values of these “robust” estimates (made from A3 sized plots of the “raw data”) are shown in Columns 2 and 3 of Table 1 for a series of 7 measurement cycles. These were the first estimates which were made (hence their designation) and were used as starting values for more precise and accurate evaluations using non-linear regression<sup>5</sup>. It is important that  $(k_R')_1$  and  $(k_R')_2$  are respectively the least precise and accurate estimates of the heat transfer coefficient which we can make from the data. They are also subject to errors due to the refilling of the cells to make up for losses in D<sub>2</sub>O due to electrolysis (see further below).

The next stage of the analysis is the evaluation of the differential lower bound heat transfer coefficient,  $(k_R')_{11}$ , throughout the time range of the measurement cycle. The subscript 11 here denotes that we are evaluating a differential coefficient and that we are considering a lower bound value. We have always used a second order central difference in the differentials of the temperature-time series. Fig. 3 shows the 11-point means,  $\overline{(k_R')_{11}}$  of  $(k_R')_{11}$  and the further 6-point means,  $\overline{\overline{(k_R')_{11}}}$ , of  $\overline{(k_R')_{11}}$  for days 1 and 2 of the measurement cycles (there was no calibration of the system during this time).

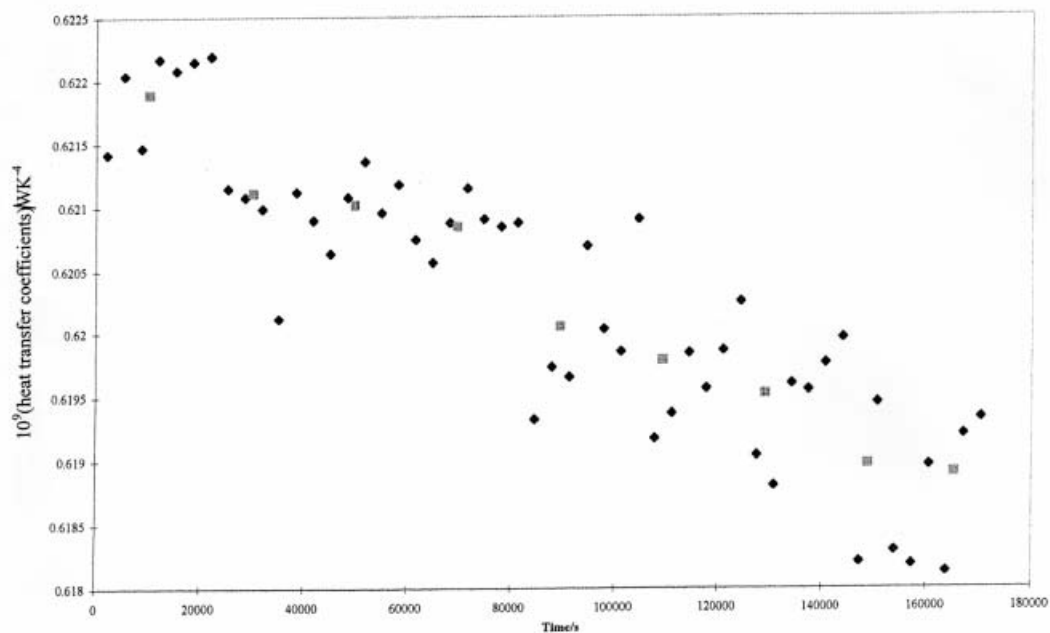


Fig 3. The values of  $\overline{(k_R')_{11}}$  ◆, and  $\overline{\overline{(k_R')_{11}}}$ , ■, for days 1 and 2 of the measurement cycles.

<sup>5</sup> In the original investigation (1), (2),  $(k_R')_2$  was estimated near  $t = t_1$ , in an attempt to eliminate one of the required interpolations. Although this procedure was explained in (2) (as was the subsequent application of non-linear regression, further explained in (6)), the basis of our estimates was clearly not understood e.g. see (7).

As we could not make the non-linear regression procedure “user friendly” with the computing power available to us in 1992, we based all further analyses on the application of linear regression (further explained in (8)). This was also the basis of the statistical treatments incorporated into the ICARUS-1 and ICARUS-2 packages (9) and is the methodology which we have adopted in all our investigations since October 1989.



We can use these coefficients in several ways to assess the performance of the instrumentation. Thus we can estimate a value of the true heat transfer coefficient from the mean of the values in Column 3, Table 1, or else, we can assume that this coefficient varies in the same way with time as does the lower bound value, Fig. 3<sup>6</sup>. We can then evaluate the differential rates of excess enthalpy generation using

$$\text{differential rate of excess enthalpy generation} = [(k_R')_2 - (k_R')_{11}] f_1(\theta) \quad (1)$$

$$\text{where } f_1(\theta) = (\text{cell temperature})^4 - (\text{bath temperature})^4 \quad (2)$$

(see also Appendix A). Fig. 4 gives the upper and lower tail distributions for Days 3-16 of the data sets (~4000 measurements) using the second set of assumptions i.e. allowing for the variation of  $(k_R')_2$  with time. We can see that the data are consistent with a normal distribution of errors (due principally to errors in the temperature measurements) on which is superimposed a small steady state rate of excess enthalpy production (due to the reduction of electrogenerated oxygen and which accounts for the positive deviations of the plots from those for a purely normal distribution of errors especially in the region of the upper tail distribution).

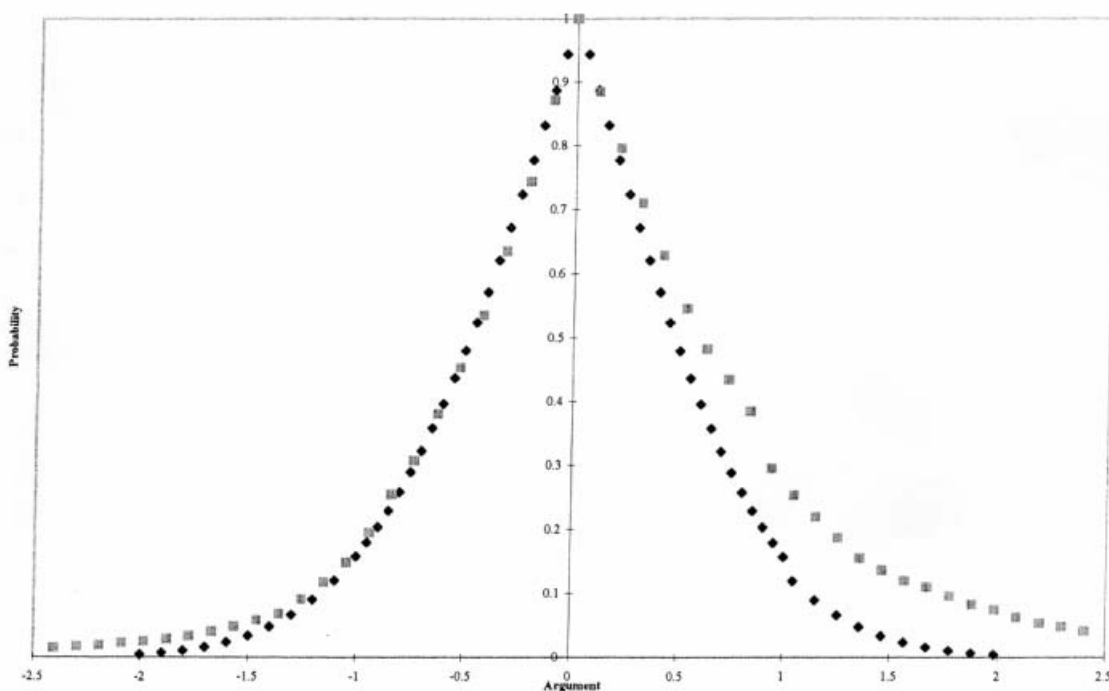


Fig 4. The upper and lower tail distributions of the differential rates of excess enthalpy generation for days 3-16 of the measurement cycles, ■; comparison with a normal distribution of errors, ◆.

We can also evaluate the corresponding rates of excess enthalpy production in a variety of ways. The methodology which we adopted in 1991-93 (and which we have also used here) is to evaluate the total excess enthalpy as a function of time and then to divide the relevant excess

<sup>6</sup> A better assumption is to base this variation on the integral heat transfer coefficient,  $(k_R')_{21}$ , Fig. 6; see further below.

enthalpy by the time elapsed since the start of the measurement cycles (here  $t = 0$  at the start of Day 3). The results for the two limiting sets of assumptions (i.e. allowing for the variation of  $(k_R')_2$  with time or else using the single value of  $(k_R')_2$  at  $t = 86,400\text{s}$ ) are given in Figs. 5A and B. We can see that the effects of the random variations in the differential lower bound heat transfer coefficient, Fig. 3, are gradually suppressed with increasing time, the rate approaching  $\sim 1.1\text{mW}$ . The significance of this value is discussed below. At the same time, we can see that the magnitudes of the excess rates given in Figs. 5A and B are affected by the assumptions made about the time dependence of the true heat transfer coefficient and that the evaluation requires very long integration intervals in order to reduce the effects of random errors to acceptable levels.<sup>7</sup>

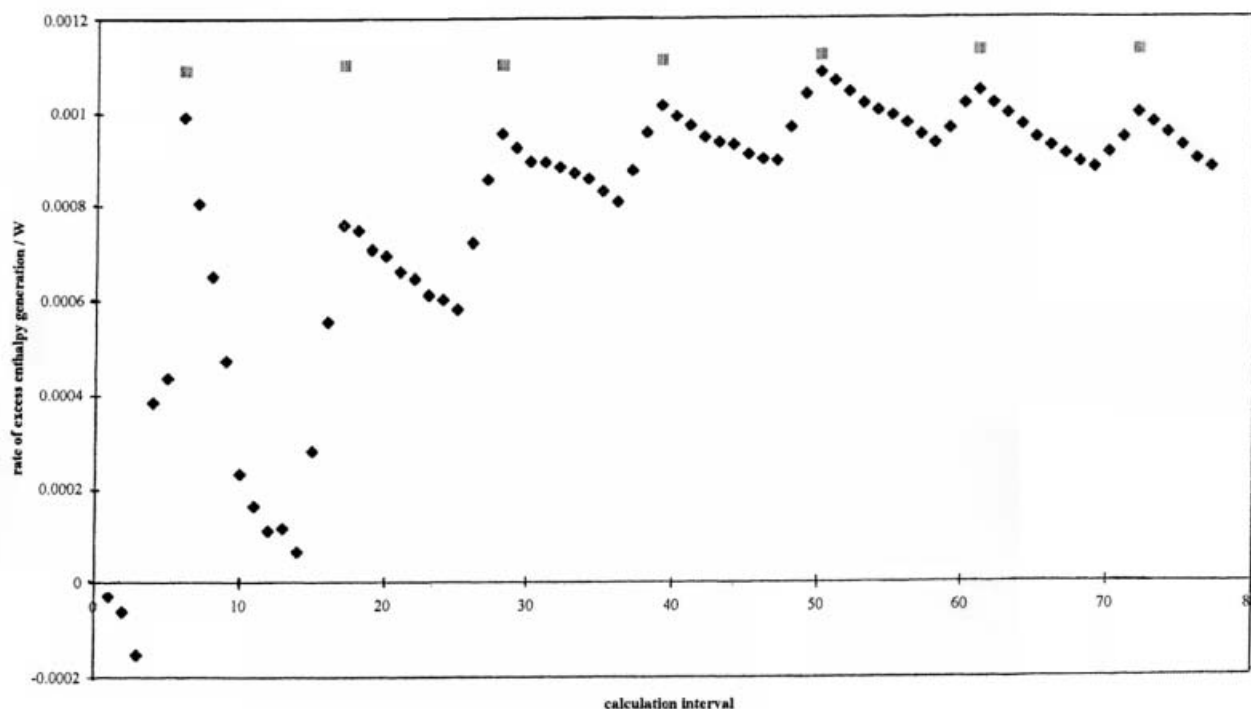


Fig 5A. The differential rates of excess enthalpy generation calculated with a true heat transfer coefficient varying with time, ◆. The figure also shows rates calculated using the integral value of the heat transfer coefficient ■, see Table 2 below.

<sup>7</sup> The evaluations carried out in 1991-93 were restricted to the first measurement cycle (with allowance for the variation of the true heat transfer coefficient with time as in Fig. 5A). This led to the erroneous conclusions that the accuracy of  $(k_R')_2$  was about one order of magnitude below the precision of  $(k_R')_1$  and that the rates of excess enthalpy production were about one tenth of the rate which could be attributed to the reduction of electrogenerated oxygen (in turn attributed to a degassing of this species from the solution adjacent to the cathode by the electrogenerated bubbles of deuterium). In fact, the accuracy of  $(k_R')_2$  must be comparable to the precision of  $(k_R')_1$ .

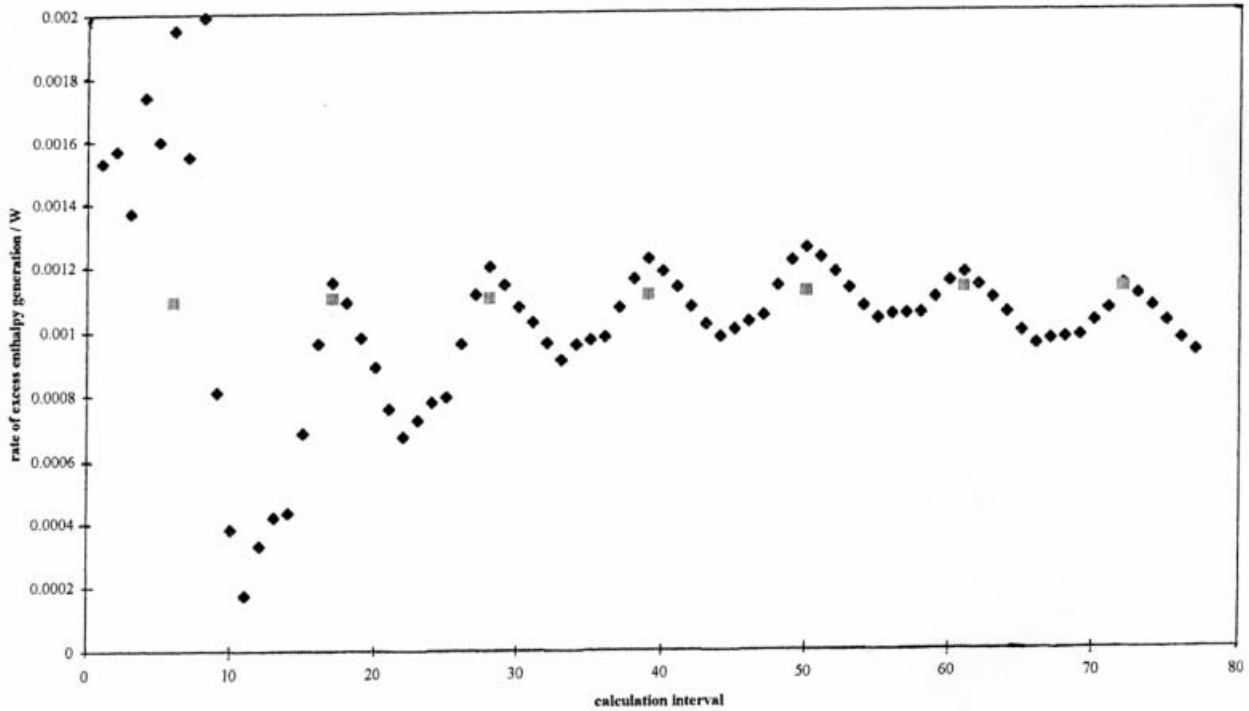


Fig 5B. the differential rates of excess enthalpy generation calculated using a single value of the true heat transfer coefficient at  $t = 86,400s$ ,  $\blacklozenge$ . The figure also shows rates Collated using the integral value of the heat transfer coefficients,  $\blacksquare$ , see Table 2 below.

The difficulties with the use of the differential heat transfer coefficient are avoided by using appropriate integral coefficients. We can distinguish two principal types denoted by the symbols  $(k_R')_{i,j,l}$  where  $i = 2$  signifies backward integration (i.e. typically starting from  $t = T$ ,  $t = t_2$  or  $t = t_1$ ),  $i = 3$  signifies forward integration (starting typically from  $t = 0$ ,  $t = t_1$  or  $t = t_2$ ),  $j = 5, 6, 7$  or  $8$  denotes the regions adjacent to  $t = 0$ ,  $t = t_1$  or  $t = t_2$  or a combination of the regions adjacent to  $t = t_1$  and  $t = t_2$  and  $l = 1$  signifies “lower bound” while  $l = 2$  signifies “true”. In this scheme of description  $i = 1$  stands for “differential” while omission of the central subscript,  $j$ , denotes that we are considering the whole measurement cycle  $0 < t < T$ . We can evidently base the evaluations on many versions of the heat transfer coefficient (which are all, of course, related to each other) so that it is necessary to standardise on the usage of a sensible subset of these coefficients.

Fig. 6 gives a comparison of the integral coefficients  $(k_R')_{21}$  (see equation A.8) and  $(k_R')_{31}$  (see equation A.9) with  $(k_R')_{11}$ . It can be seen that if we exclude the first  $\sim 100$  data points adjacent to  $t = T$  in the evaluation of  $(k_R')_{21}$  and the first  $\sim 100$  data points adjacent to  $t = 0$  in the evaluation of  $(k_R')_{31}$  (time zones in which the benefits of the integral procedure are established), the variability of  $(k_R')_{21}$  and  $(k_R')_{31}$  is actually much smaller than that of  $(k_R')_{11}$ .

The interrelation of these coefficients can be understood as follows:

the variation of  $(k_R')_{11}$  with time can be represented to the first order by

$$(k_R')_{11} = (k_R')_{11}^0 (1 - \gamma t) \quad (3)$$

where  $(k_R')_{11}^0$  is the value of  $(k_R')_{11}$  at  $t = 0$ . If the time dependence of the heat transfer coefficients is included in the differential equation (A.1) representing the calorimeter, we obtain for example, equation (A.13). If we now regard  $f_1(\theta)$  as being constant throughout a measurement cycle (which

is a rough approximation for the case of the “lower bound heat transfer coefficients” in the absence of a calibration pulse) we obtain

$$(k_R')_{21} = (k_R')_{21}^0 [1 + \frac{\gamma(T-t)}{2}] \quad (A.14)$$

and

$$(k_R')_{31} = (k_R')_{31}^0 [1 - \frac{\gamma t}{2}] \quad (A.15)$$

where  $(k_R')_{21}^0$  and  $(k_R')_{31}^0$  are respectively the values of  $(k_R')_{21}$  and  $(k_R')_{31}$  at  $t = T$  and  $t = 0$ . It follows that the slopes of the plots of  $(k_R')_{21}$  and  $(k_R')_{31}$  versus time are roughly one half of the corresponding plot of  $(k_R')_{11}$  and hence those for  $\overline{(k_R')}_{11}$  and  $\overline{(k_R')}_{11}$  as is shown by Fig. 6.

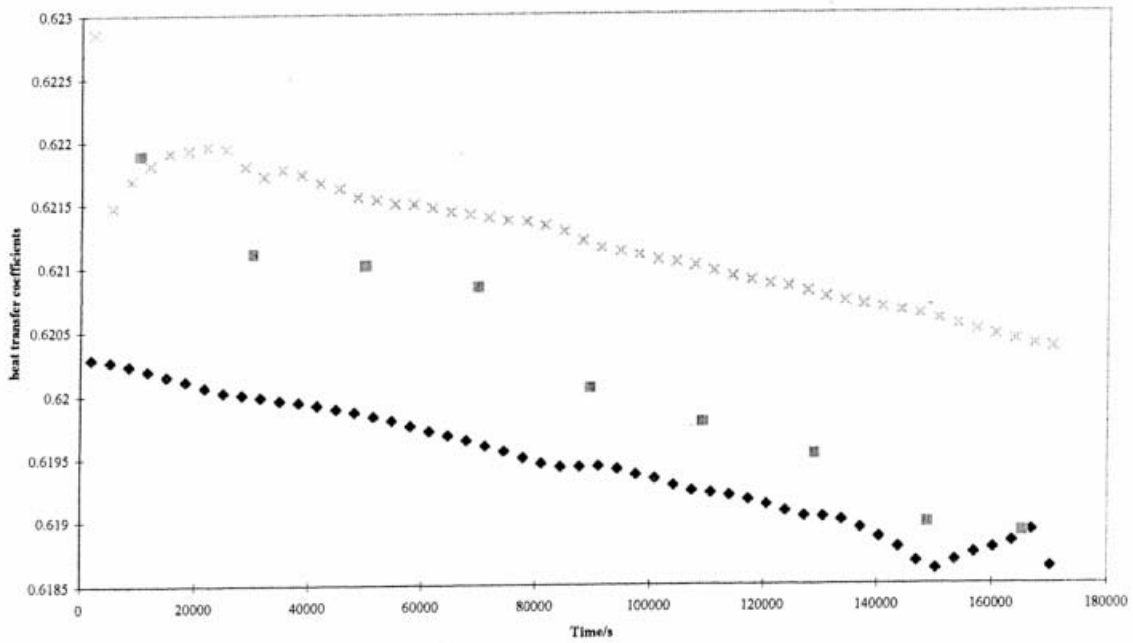


Fig. 6. Comparison of the variation with time of the integral heat transfer coefficients,  $(k_R')_{31}$  and  $(k_R')_{21}$   $\times$ ,  $\blacklozenge$ , with the differential lower bound heat transfer coefficient,  $\overline{(k_R')}_{11}$   $\blacksquare$ . Days 1 and 2 of the measurement cycles.

An alternative approach towards the evaluation of accurate values of the heat transfer coefficients can be based on the application of equations such as (A.8), (A.9), (A.11) and (A.12). Such evaluations give  $(k_R')_{i,j,l}^0$ , which are the intercepts at the chosen origins of the abscissae of  $C_p M d(\Delta\theta)/dt$ , (note that these intercepts are independent of the value of  $C_p M$ ); the water equivalents are derived from the slopes of the plots.

Figs. 7A,7B and 8 illustrate the determination of  $(k_R')_{261}^0$  and  $(k_R')_{262}^0$  with the start and end of the integration procedures being set at  $t = t_2$  and  $t = t_1$ , (for Figs. 7A and 8) and  $t = T$  and  $t = t_1$ , for Fig. 7B. It should be noted that the origin for the plots in Figs. 7A and 8 is well-defined near  $t = t_2$  (where  $d\Delta\theta/dt \sim 0$ ) which is the point in time at which we require the heat transfer coefficients. The small values of the abscissae should be especially noted as should the degradation of the performance when setting the origin at  $t = T$  (Fig. 7B) compared to  $t = t_2$  (Fig. 7A) The evaluation of these heat transfer coefficients became one of the targets of the ICARUS procedures; the values determined for these sets of measurements are listed in Columns 4-7 of Table 1. The values of

$(k_R')_{261}^0$  determined in this way, Column 4 of Table 1, are somewhat larger than the values of  $(k_R')_{21}$  determined at the same point in time listed in Column 8. This is expected as the extrapolations determine  $(k_R')_{11}$  at  $t = t_2$  (rather than  $(k_R')_{21}$ ). We would expect that the means of  $(k_R')_{261}^0$  and  $(k_R')_{262}^0$  (Columns 4 and 6 of Table 1) to be close to the means of  $(k_R')_1$  and  $(k_R')_2$  (Columns 2 and 3 of Table 1). Table 1 shows that this is indeed the case.

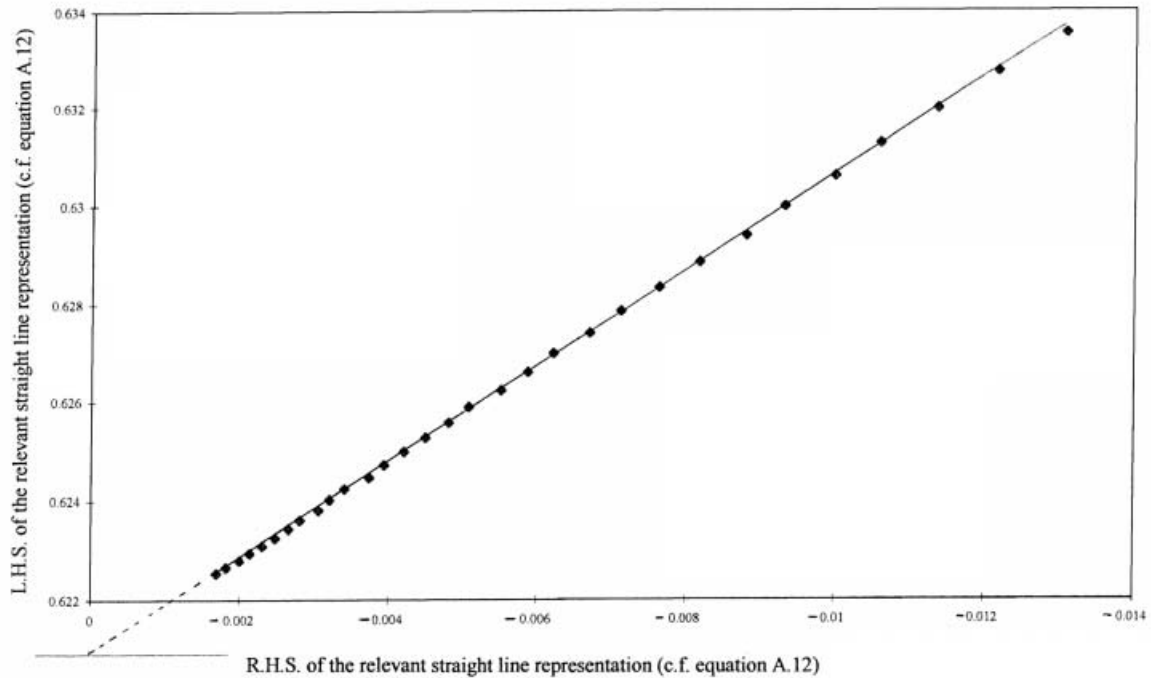


Fig 7A. Evaluation of  $(k_R')_{261}^0$  and CpM for Days 9 and 10 of the measurement cycles. Origin of the integrations set at  $t=t_2$ .

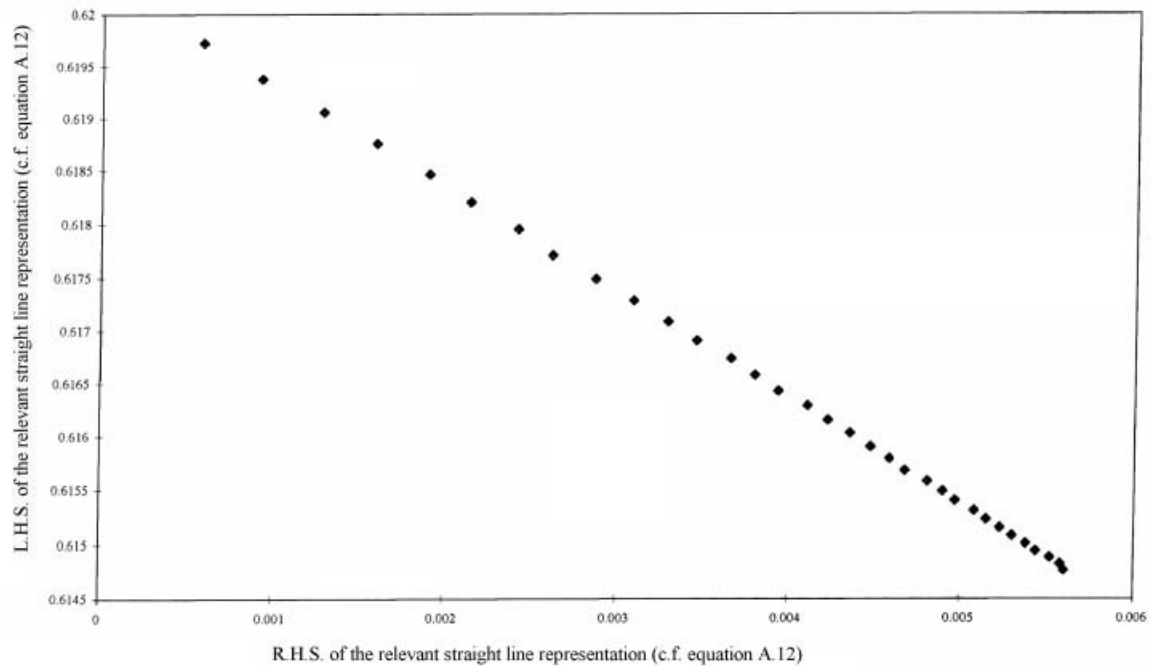


Fig 7B. Evaluation of  $(k_R')_{261}^0$  and CpM for Days 9 and 10 of the measurement cycles. Origin of the integrations set at  $t=T$ .

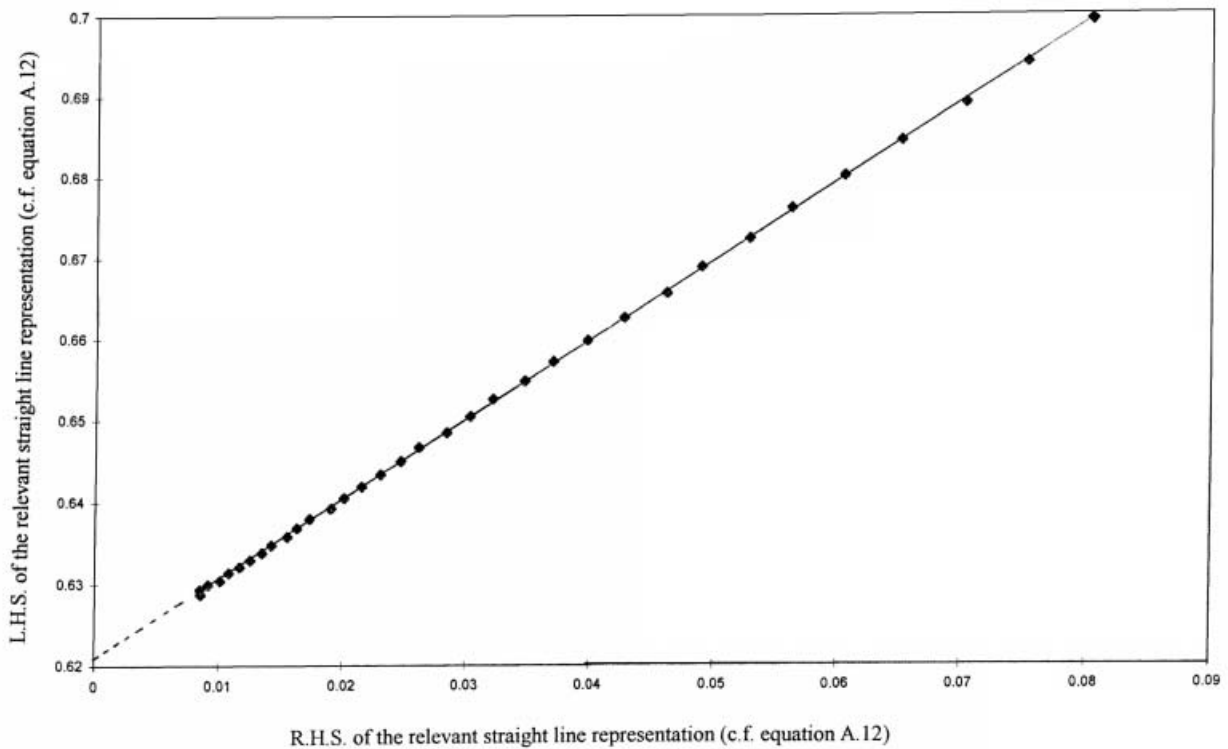


Fig 8. Evaluation of  $(k_R')_{262}^0$  and  $C_pM$  for Days 9 and 10 of the measurement cycles. Origin of the integrations set at  $t=t_2$ .

Columns 9-12 of Table 1 list the values of  $(k_R')_{361}^0$  and  $(k_R')_{362}^0$  (and the associated values of the water equivalents and statistics) based on the forward integration of the data from  $t = t_1$ . Such evaluations are unsatisfactory from several points of view. In the first place, the origin of the plots required for the derivation of these coefficients is not well defined ( $d\Delta\theta/dt \neq 0$  as  $t \rightarrow t_1$ ); secondly, the range of the extrapolations is too long; thirdly, the values of the abscissae are large and comparable to the ordinates. It is not surprising therefore that the determination of the heat transfer coefficients using these particular procedures fails (see Columns 9-12 of Table 1). It was pointed out that evaluations near the end of the calibration pulse would be more satisfactory than those close to the start of this pulse,  $t = t_1$ , as can be seen from a comparison of Columns 13-16 with 9-12 of Table 1. As the time at which the derived heat transfer coefficients might apply was uncertain, the procedures based on the forward integration of the data sets was excluded from the ICARUS Systems<sup>8</sup>. However, the evaluation of  $(k_R')_{31}$  near  $t = t_2$ , Column 17 of Table 1, was included to serve as a check on the procedures.

It is important to point out a major limitation of these analyses. It can be seen that the time-dependence of the evaluated coefficients (e.g. see Figs. 3 and 6) is entirely in accord with the expected behaviour, equations (A.1) and (A.2). It was therefore hoped that the derived values of  $C_pM$  could be used to provide the minor corrections to the level of the electrolyte to allow the presentation of the derived heat transfer coefficients on a single plot versus the electrolyte content of the cells. However, this objective could never be realised. The water equivalents are derived from the slopes of the plots such as those in Figs. 7A-8. Inevitably, this introduces errors into the estimates of  $C_pM$  and the accuracy of the heat transfer coefficients is insufficient to allow the

<sup>8</sup> However, we believe that the evaluations carried out by the group at the New Hydrogen Energy Laboratories have been based on such forward integrations.

correction of the heat transfer coefficients for changes in the electrolyte level between successive measurement cycles.<sup>9</sup>

In the full text of the paper dealing with this subject (10) we have covered additionally;

- (i) the response of the system following the “topping up” of the cells to make up for losses of D<sub>2</sub>O due to electrolysis in the previous measurement cycle (rather than the responses due to the calibration pulse). We have shown that the heat transfer coefficients  $(k_R')_{251}^0$  and  $(k_R')_{252}^0$  have only limited accuracy using the methodology as currently developed; however, this approach requires further investigation;
- (ii) the evaluation of  $(k_R')_{271}^0$ ; however, the determination of the heat transfer coefficient at  $t = T$  was not of any particular significance and this particular evaluation was not included in the data evaluation package (9);
- (iii) assessments of the errors in the various evaluations of the heat transfer coefficients. It was shown that the assessment of errors in the integral heat transfer coefficients can become limited by the cut-off limit of the interpretation i.e. if the errors are less than  $\pm 0.00001 \times 10^9 (k_R')$ .<sup>10</sup>

In common with other investigations (e.g. see (2), (8)) it was observed that the relevant standard deviations are so small that it should be possible to make thermal balances to within 0.1mW for a typical input of 1W. The analysis presented here shows that such balances should be made using the integral heat transfer coefficients  $(k_R')_{22}$  estimated at  $t = 0$ . Table 2 illustrates such a calculation made using the seven applicable measurement cycles. The rate of excess enthalpy generation shown in Column 8 is 0.0011W and these rates are also shown in Figs. 5A and B in comparison with those calculated using the differential heat transfer coefficients  $(k_R')_{12}$ . These rates, are approximately equal to the rates which may be calculated for the reduction of electrogenerated oxygen present in the cell (compare (12)). It will be clear that we must regard these rates as being constant during each measurement cycle, an assumption which is evidently justified. The data shown in Column 8 of Table 2 confirm that such rates can be estimated to within  $\pm 0.0001$ W which requires that the accuracy of the true integral heat transfer coefficient must be nearly equal to the precision of the lower bound values i.e. that the errors are  $\pm 0.01\%$ .

---

<sup>9</sup> A level controller was added to the ICARUS-2 instrumentation and it was estimated that this would reduce the errors in the heat transfer coefficients to  $\pm 0.04\%$ . However, these level controllers were never used. Level controllers for the water baths surrounding the calorimeters were also never constructed. The ICARUS-2 system was also designed to use the cell currents to drive the calibration heaters (so as to remove all possibility of errors introduced by differences in the power outputs delivered to the cell and calibration heaters). However, this modification of the experiment was never used.

<sup>10</sup> It was noted that the individual values of the integral heat transfer coefficients are not statistically independent as the process of integration uses all the preceding values of the raw data. A method of avoiding this difficulty by sectioning the data sets was illustrated (10).

Table 2									
Thermal balances using the integral heat transfer coefficient based on backward integration of the data sets.									
1	2	3	4	5	6	7	8		
Days	input dt	$10^{-9} f_1(0)dt$	$10^9(k_R')_{262}$	$10^9(k_R')_{262}$	thermal	output -	equivalent		
	/J	$K^4s$	/WK <sup>-4</sup>	/WK <sup>-4</sup>	output	input dt	excess rate		
			near t=t <sub>2</sub>	near t=0	/J	/J	/W		
3 and 4	140501.14	226640.24	0.6187	0.6195	140403.63	181.313	0.00109		
5 and 6	141848.96	228529.44	0.62034	0.62114	141948.78	182.824	0.00110		
7 and 8	141774.43	228484.27	0.62021	0.62101	141891.02	182.788	0.00110		
9 and 10	143166.58	230672.08	0.61995	0.62075	143189.69	184.538	0.00111		
11 and 12	143956.74	231844.19	0.62043	0.62123	144028.57	185.476	0.00112		
13 and 14	145003.77	233772.4	0.62011	0.62091	145151.59	187.018	0.00113		
15 and 16	144858.04	233584.78	0.61974	0.62054	144948.7	186.868	0.00113		

## Discussion

The material presented in this paper shows that exact data analyses should be based on the evaluation of the true integral heat transfer coefficient,  $(k_R')_{22}$  coupled to the integral lower bound heat transfer coefficient,  $(k_R')_{21}$ . Accurate and precise estimates of these coefficients can be obtained from  $(k_R')_{262}^0$  and  $(k_R')_{261}^0$ , the values which apply to the calibration period  $t_1 < t < t_2$ . The procedure which has been illustrated here was part of that incorporated into the ICARUS-System methodology (9).

The accuracy of  $(k_R')_{22}$  and the precision of  $(k_R')_{21}$  are very nearly equal with errors of  $\sim \pm 0.01\%$ . Such errors can in fact be estimated from the errors in the temperature measurements coupled to the averaging procedures described in this paper. The precision and accuracy which can be achieved should be compared to the rather wild statements which have been made in the literature about the accuracy of this type of instrumentation. Such statements can be seen to be the outcome of inadequate experiments coupled to inadequate and incomplete interpretations.

It will be seen that the application of the integral heat transfer coefficients requires that the rates of any excess enthalpy generation be constant in time. In turn, this requires that the experiments be carried out using suitable "blank systems". If the rates of excess enthalpy generation vary with time, we will inevitably conclude that the instrumentation has enhanced errors. Moreover, such a conclusion will apply to any calorimetric system which we might propose. The lack of execution of "blank experiments" is undoubtedly a contributory factor to the confusing statements which have been made in the literature.

The wild statements which have been made in the literature extend also to the effects of the reduction of electrogenerated oxygen. These rates can be estimated perfectly adequately by carrying out suitable "blank experiments". We note that if the precision and accuracy of the instrumentation is lowered to say  $\pm 1\%$ , it will then be impossible to measure such rates; equally, it will be impossible to monitor the build-up of excess enthalpy generation until this has reached specific rates in the range  $0.1-1 \text{ Wcm}^{-3}$ . Such deficiencies are no doubt at the root of many of the further confusing results and statements which have been made in the literature. In this connection we note that correctly designed isoperibolic calorimeters should be classified as "ideal reactors" using the nomenclature of Chemical Reaction Engineering (13). While it would be possible to design other

types of reactor (such as flow reactors) to satisfy the criteria of “ideal plug flow”, such research has only recently been initiated (14). Existing designs fall under the heading of “dispersive plug flow” and such designs are undoubtedly non-ideal.

We observe also that the calibration of the cells could be based equally well on the determination of the lower bound heat transfer coefficients for suitable “blank experiments”. The use of such coefficients in the data analysis for Pd-based cathodes in D<sub>2</sub>O-based electrolytes would then automatically discriminate against the contribution of the reduction of electrogenerated oxygen to the total rates of excess enthalpy generation.

## References

- 1) M. Fleischmann, S. Pons and M. Hawkins, J. Electroanal. Chem., 261 (1989) 301; 263 (1989) 187.
- 2) M. Fleischmann, S. Pons, M.W. Anderson, L. J. Li and M. Hawkins, J. Electroanal. Chem., 287 (1990) 293
- 3) Frederick T. Wagner, Thomas E. Moylan, Michael E. Hayden, Ulrike Narger and James L. Booth, J. Electroanal. Chem., 295 (1990) 393.
- 4) Wilford N. Hansen, Proceedings of the Second Conference on “Cold Fusion”, Conference Proceedings of the Italian Physical Society, Bologna; Editors: Tullio Bressani, Emilio Del Giudice and Giuliano Preparata, 33 (1991) 491 ; ISBN 88-7794-045-X.  
See also Michael E. Melich and Wilford N. Hansen, Proceedings of the Third International Conference on “Cold Fusion, Universal Academy Press, Frontiers of Science Series No 4 Tokyo ; Editor H. Ikegami (1993) 397 ; ISBN 4-946493-12-6.
- 5) Wilford N. Hansen, see this Meeting.
- 6) M. Fleischmann and S. Pons, J. Electroanal. Chem., 332 (1992) 33.
- 7) R. H. Wilson, J. W. Bray, P. G. Kosky, H. B. Vakil and F. G. Will, J. Electroanal. Chem., 332 (1992) 1.
- 8) M. Fleischmann, S. Pons, Monique Le Roux and Jeanne Roulette, Trans. Fusion Technol., 26 (1994) 323.
- 9) The ICARUS Systems; Isoperibolic Calorimetry: Acquisition, Research and Utilities System, Version 1 (December 1993), Low Power Measuring System for Three Cells, Technova Inc., 13<sup>th</sup> Floor, Fukoku Seimei Building, 2-2-2 Uchisaiwai-cho, Chiyoda-Ku, Tokyo 100, Japan.  
  
ICARUS -2 ; Isoperibolic Calorimetry : Acquisition, Research and Utilities System. Document Version 2.0 (February 1995). Technova Inc., 13<sup>th</sup> Floor, Fukoku Seimei Building, 2-2-2 Uchisaiwai-cho, Chiyoda-Ku, Tokyo 100, Japan.
- 10) M. Fleischmann and M. H. Miles, “Our Penultimate Papers on the Isoperibolic Calorimetry of the Pt/D<sub>2</sub>O Systems ; Part I : the Pt/ D<sub>2</sub>O Blank System”, submitted for publication.
- 11) Martin Fleischmann and Stanley Pons in Editor H. Ikegami, “Frontiers of Cold Fusion” Proceedings of the Third International Conference on Cold Fusion,

Universal Academy Press, Tokyo, 100-91, Japan, Frontiers of Science Series No 4  
ISSN 0915-8502, ISBN 4-946443-12-6 (1993), 47.

- 12) Fritz G. Will, *J. Electroanal. Chem.*, 426 (1997) 177.
- 13) O. Levenspiel, "Chemical Reaction Engineering" (1972) John Wiley, London.
- 14) M.H. Miles, see this Meeting.
- 15) M.H. Miles, M. Fleischmann and M.A. Imam, Report NRL/MR/6320-01-8526,  
Naval Research Laboratory, Washington, DC 20375-5320, March 2001.
- 16) S. Szpak and P.A. Mosier-Boss, Technical Report, Volume 2, SPAWAR Systems  
Centre, San Diego, February 2002.

## Appendix

It has been established that at low to intermediate cell temperatures (say  $30^\circ < \theta < 80^\circ$ ) the behaviour of the calorimeters is modelled adequately by the differential equation

$$\begin{aligned}
 C_p M (d\Delta\theta/dt) &= [E_{\text{cell}}(t) - E_{\text{thermoneutral,bath}}]I + Q_f(t) \\
 \text{change in the enthalpy content} & \quad \text{enthalpy input due to} & \quad \text{rate of excess enthalpy} \\
 \text{of the calorimeter} & \quad \text{electrolysis} & \quad \text{generation} \\
 \\
 +\Delta QH(t-t_1) - \Delta QH(t-t_2) - & (3I/4F[P/\{P^*-P\}][C_{p,D_2O,g} - C_{p,D_2O,l}]\Delta\theta + L] \\
 \text{calibration pulse} & \quad \text{rate of enthalpy removal by the gas stream with} \\
 & \quad E_{\text{thermoneutral}} \text{ referred to the bath temperature} \\
 \\
 - (k_R^0)\theta_{\text{bath}}^3[1-\gamma t] & \quad \{f_1(\theta)/\theta_{\text{bath}}^3 + 4\phi\Delta\theta\} \\
 \text{time dependent} & \quad \text{effect of} & \quad \text{effect of conduction} \\
 \text{heat transfer} & \quad \text{radiation} & \\
 \text{coefficient} & & 
 \end{aligned} \tag{A.1}$$

With the calorimeters supplied with the ICARUS Systems, the conductive contribution to heat transfer is very small. This term could therefore be “lumped” into the radiative term by allowing for a small increase in the radiative heat transfer coefficient:

$$\text{Radiative heat transfer} = (k_R')^0 [1-\gamma t] [(\theta_{\text{bath}} + \Delta\theta)^4 - \theta_{\text{bath}}^4] \tag{A.2}$$

The values of the pseudoradiative “heat transfer coefficient,  $(k_R')^0 [1-\gamma t]$ , derived are close to those calculated from the Stefan-Boltzmann coefficient and the radiative surface area. If the time dependence of the heat transfer coefficient is not included explicitly in equation (A.2) then

$$\text{Radiative heat transfer} = (k_R') [(\theta_{\text{bath}} + \Delta\theta)^4 - \theta_{\text{bath}}^4] \tag{A.3}$$

where the pseudoradiative heat transfer coefficient,  $(k_R')$ , now shows a weak time-dependence.

The simplest starting point is to assume that there is no excess enthalpy generation in the calorimeter and to evaluate a corresponding “differential lower bound heat transfer coefficient” at a time just before the end of the calibration pulse,  $t = t_2$  :

$$(k_R')_1 = [(E_{\text{cell}}(t) - E_{\text{thermoneutral,bath}})I - \Delta H_{\text{evap}}(t) - C_p M (d\Delta\theta/dt) + \Delta QH(t-t_1)] / f_1(\theta) \tag{A.4}$$

This was the first heat transfer coefficient used in our investigations, hence the designation  $(k_R')_1$ . It will be apparent that the differential lower bound heat transfer coefficient  $(k_R')_{11}$ , may be evaluated at other points of the measurement cycle, by changing the enthalpy input due to the calibration pulse to

$$\Delta QH(t-t_1) - \Delta QH(t-t_2) \tag{A.5}$$

It is next necessary to evaluate a “true heat transfer coefficient”. The simplest procedure giving  $(k_R')_2$  near the end of the calibration period at  $t=t_2$  is obtained by including the calibration pulse

$$(k_R')_2 = \{ \Delta Q + [E_{\text{cell}}(\Delta\theta_2, t_2) - E_{\text{cell}}(\Delta\theta_1, t_2)] I - \Delta H_{\text{evap}}(\Delta\theta_2, t_2) + \Delta H_{\text{evap}}(\Delta\theta_1, t_2) - C_p M [(d\Delta\theta/dt)_{\Delta\theta_2, t_2} - (d\Delta\theta/dt)_{\Delta\theta_1, t_2}] \} / f_2(\theta) \quad (\text{A.6})$$

where we now have

$$f_2(\theta) = [\theta_{\text{bath}} + (\Delta\theta_2, t_2)]^4 - [\theta_{\text{bath}} + (\Delta\theta_1, t_2)]^4 \quad (\text{A.7})$$

It can be seen that we need to estimate the cell potential, the cell temperature and the differential of this temperature at the time  $t=t_2$  which would have been reached in the absence of the calibration pulse [see footnote (A.1)]<sup>A1</sup>

As is explained in the main text, it is preferable to base the evaluation of the “raw data” on the integrals of the enthalpy input and of the temperature functions rather than to lower the precision and accuracy of the evaluations by using the differentials of the inherently noisy temperature-time series.

For the backward integrals starting from  $t \approx T$  we obtain

$$(k_R')_{21} = \frac{\int_T^t \text{net enthalpy input}(\tau) d\tau}{\int_T^t f_1(\theta) d\tau} - \frac{C_p M [\Delta\theta(t) - \Delta\theta(T)]}{\int_T^t f_1(\theta) d\tau} - \frac{Q_f [t - T]}{\int_T^t f_1(\theta) d\tau} \quad (\text{A.8})$$

while forward integration from the start of the measurement cycle

$$(k_R')_{31} = \frac{\int_0^t \text{net enthalpy input}(\tau) d\tau}{\int_0^t f_1(\theta) d\tau} - \frac{C_p M [\Delta\theta(t) - \Delta\theta(0)]}{\int_0^t f_1(\theta) d\tau} - \frac{Q_f [t]}{\int_0^t f_1(\theta) d\tau} \quad (\text{A.9})$$

The evaluation of the heat transfer coefficients applicable to particular time regions ( $j = 5, 6, 7, 8$ ) simply requires changes in the lower limits of the relevant integrals.

The evaluation of the “true heat transfer coefficients” requires the combination of the enthalpy inputs in equations (A.8) and (A.9) with the thermal inputs made at one or a series of

---

<sup>A1</sup> This evaluation was carried out in a somewhat different manner in the initial studies (1), (2) (10) in an attempt to avoid the disadvantages of such interpolation procedures. The values of  $(k_R')_{11}$  and  $(k_R')_2$  obtained were used as starting values for the non-linear regression procedure used at that time (2). As we could not make this procedure “user friendly” with the computing power then available to us and as, more especially, the methodology which we adopted was evidently not understood (7). (for a further example of such misunderstanding see (3) ) we adopted the methodology described in the present paper. This methodology was also the basis of the ICARUS Systems (9).

points. This can be carried out in a number of ways; we confine attention here to the procedure originally suggested in the Handbook for the ICARUS - 1 System (9). If we consider  $(k_R')_{362}$  and if we make a thermal balance just before the application of the calibration pulse, then if the system has relaxed adequately so that we can set  $d\Delta\theta/\approx 0$

$$0 = [\text{Net enthalpy input}(t_1)][t - t_1] + Q_f[t - t_1] - (k_R')_{32} \{[(\theta_{\text{bath}} + \Delta\theta(t_1))^4 - \theta_{\text{bath}}^4]\} [t - t_1] \quad (\text{A.10})$$

Combination with equation (A.9) (with the appropriate change in the lower limit of the integration) gives

$$\left(k_R'\right)_{362} = \frac{\int_{t_1}^t \text{net enthalpy input}(\tau) d\tau - [\text{net enthalpy input}(t_1)][t - t_1] - C_p M [\Delta\theta(t) - \Delta\theta(t_1)]}{\int_{t_1}^t f_1(\theta) d\tau} \quad (\text{A.11})$$

The corresponding equation for  $(k_R')_{262}$  follows from (A.11) on replacing  $t_1$  by  $t_2$ . It is convenient to write all the equations for the determination of the relevant heat transfer coefficients in the “straight line form” e.g.

$$\frac{\int_{t_2}^t \text{net enthalpy input}(\tau) d\tau - [\text{net enthalpy input}(t_1)][t - t_2]}{\int_{t_2}^t f_1(\theta) d\tau} = \frac{C_p M [\Delta\theta(t) - \Delta\theta(t_2)]}{\int_{t_2}^t f_1(\theta) d\tau} + \left(k_R'\right)_{262}^{\circ} \quad (\text{A.12})$$

where  $(k_R')_{262}^{\circ}$  can be seen to be the value of the integral heat transfer coefficient at  $t = t_2$ . The value of  $t_2$  should be chosen to be the mid-point of the measurement cycle as  $(k_R')_{262}^{\circ}$  is the most useful (and well defined) value of the true heat transfer coefficient. It should be noted that extrapolations such as (A.12) automatically remove the effects of  $C_p M$  on the value of the derived heat transfer coefficient (a desirable feature because the water equivalents of the cells have the highest errors).

The integral lower bound heat transfer coefficient,  $(k_R')_{261}^{\circ}$  (equation (A.8) with  $T$  replaced by  $t_2$ ) and the integral true heat transfer coefficient,  $(k_R')_{262}^{\circ}$ , (equation (A.12)) were the “target procedures” for the ICARUS -style evaluations of the experimental data (9).

It should be noted that the definitions of the integral heat transfer coefficients given in this Appendix have regarded these coefficients as being constant in time whereas we would,

in fact, anticipate a weak time dependence e.g. equation (A.2) or Fig. 6. This weak time-dependence causes an equally weak time-dependence of the derived heat transfer coefficients. Use of the more exact equation (A.2) gives for example for the derived values of  $(k_R')_{21}$  in (A.8)

$$(k_R')_{21} = (k_R')_{21}^0 [1 - \gamma(t-T) + \gamma \int_T^t \int_T^t f_1(\theta) d\tau d\tau / \int_T^t f_1(\theta) d\tau] \quad (\text{A.13})$$

where  $(k_R')_{21}^0$  is the value of  $(k_R')_{21}$  at  $t = T$ . An ultimate test of the validity of the representation of the calorimeters by the differential equation (A.1) is therefore the question of whether the heat transfer can be represented by a single time-dependence coefficient, here  $(k_R')_{21}^0$ . This question is discussed further in the main text.

We also note that if we regard  $f_1(\theta)$  as being constant throughout the measurement cycle (which is a rough approximation for the case of the “lower bound heat transfer coefficients”) then (A.13) becomes

$$(k_R')_{21} = (k_R')_{21}^0 [1 + \gamma(T - t)/2] \quad (\text{A.14})$$

Similarly, we obtain

$$(k_R')_{31} = (k_R')_{31}^0 [1 - \gamma t/2] \quad (\text{A.15})$$

where  $(k_R')_{31}^0$  is now the value of  $(k_R')_{31}$  at  $t = 0$ . It follows that the slopes of the plots of  $(k_R')_{21}$  and  $(k_R')_{31}$  versus time are roughly one half of the plot of  $(k_R')_{11}$  versus time (cf. Fig. 6)

For a more complete discussion see (15), (16).